Sigma J Eng & Nat Sci 36 (3), 2018, 609-618

Sigma Journal of Engineering and Natural Sciences
Sigma Mühendislik ve Fen Bilimleri Dergisi

Research Article

THE SPREADING PROFILE OF AN IMPINGING LIQUID JET ON THE HYDROPHOBIC SURFACES

Ali KİBAR*[1], Kadri Süleyman YİĞİT[2]

[1]*Dept. of Mechanical and Material Tech., Kocaeli University, KOCAELI;* ORCID:0000-0002-2310-1088
[2]*Department of Mechanical Engineering, Kocaeli University, KOCAELI;* ORCID:0000-0003-1277-9405

Received: 14.12.2017 Revised: 28.02.2018 Accepted: 06.03.2018

ABSTRACT

In this study, the spreading profiles of the impinging liquid jets on the superhydrophobic/hydrophobic surfaces have been examined experimentally and predicted using experimental data. The liquid jet is sent on the flat and smooth hydrophobic surfaces, which have 93, 104 and 117° contact angles, using the glass tube nozzle with the 1.75 mm inner diameter. The inclination angles between the jet and surface are altered in the range of 15-45°. The predicted profiles compared with the experimental data. The spreading behaviour of the impinging liquid jet on the hydrophobic surface is clarified using the predicted equation. The inclination angle is a dominant parameter for the profile of the spreading liquid. The predicted equation is in a good agreement with the experiments. The front length of the spreading liquid takes the maximum value at a critical inclination angle.
Keywords: Liquid jet, hydrophobic surface, spreading profile, impinging jet.

Nomenclature

Roman

L_r : rear length of jet spreading profile (m)
L_f : front length of jet spreading profile (m)
r_0 : radius of jet (m)
r_ψ : polar radius (m)
v_{jet} : velocity of jet (m s^{-1})
W : width of the spreading liquid (m)
Re : Reynolds number of jet = $2r_0\rho v_{jet}/\mu$ (dimensionless)
We : Weber number of jet = $2r_0\rho v_{jet}^2/\gamma$ (dimensionless)

Greek

α : inclination angle of jet to the surface (°)
γ : surface tension (N m^{-1})
θ : contact angle (°)
μ : dynamic viscosity (Pa s)
ρ : density (kg m^{-3})
ψ : azimuthal angle of jet spreading profile along the flow (°)

* Corresponding Author: e-mail: alikibar@kocaeli.edu.tr, tel: (262) 351 34 82

1. INTRODUCTION

Liquid jets impinging on the solid surfaces have been widely used for industrial processes and applications such as cooling, cleaning, coating, and ink-jet printing [1]. The characteristic of flow is important for these processes. Besides the characteristic of flow, the flow patterns formed by impinging jet should be also well known [2].

When a vertical liquid jet impinges on a horizontal solid surface, the liquid spreads radially as a thin film. The velocity of flow in thin film is high and the thickness of the film increases abruptly at a certain distance from the impingement zone. Therefore, the thin film is bounded with a circular and thick flow. This phenomenon is called as circular hydraulic jump [3].

The spreading behaviour of the impinging liquid jet is widely altered with respect to the features of the surface and jet. For example, the contact angle of the surface and the inclination angle of the jet are some of the dominant parameters for the spreading behaviour of the impinging jet. The impinging of a vertical liquid jet does not continue its way on the horizontal superhydrophobic surface as a thin film flow and liquid breaks up as droplets after the thin film [4]. If the angle between the jet and the superhydrophobic surface is not perpendicular, the liquid jet reflects from the surface after spreading a certain area owing to stored surface energy of the spreading liquid [5]. The spreading area increases with decrease in contact angle which results in the surface energy decreases [6–8]. Therefore, the liquid jet may not get sufficient energy for reflection and it flows several consecutive spreading on the hydrophobic surface, called as braiding type flow [9].

Mertens et al. [9] introduced a theoretical model for spreading profile of the consecutive braiding flow pattern on the flat hydrophilic surface. Kibar et al. [5] examined an impingement of an oblique liquid jet on the hydrophobic and superhydrophobic surfaces. They classified the spreading behaviour of the liquid jet on the solid surface dependent on mainly the contact angle of the surface; those were the reflection, braiding, splashing types flow. Kibar [6] performed the experimental and numerical studies for spreading of the impinging liquid jet on a superhydrophobic surface by considering the energy transformation between the liquid jet and spreading liquid, and between spreading liquid and reflection jet, respectively. In that study, the stored surface energy of the spreading liquid was considered in both the 2D and 3D. It was pointed out that the rate of the surface area of the spreading liquid to wetted area was a dominant factor for stored surface energy, which was mainly affected by the contact angle [6].

The opposite impinging liquid jets in air resemble the impinging of the oblique liquid jet on the hydrophobic surface; in contrast there is no liquid-solid interaction. In the case of impinging liquid jet on the hydrophobic surface, the spreading of the liquid is affected by not only the internal dissipation in the flow, but also frictional force against the wall, and the capillary force is another factor for the spreading at the three phase contact line with respect to the contact angle. There have been numerous experimental and theoretical studies about the profile of the impinging opposite liquid jets such as [10–12].

Figure 2 shows an illustration of an impinging liquid jet on a hydrophobic surface at an inclination angle (α). The impingement region is the section of the jet on the plane parallel to the surface as an elliptical shape of major axis ($2r_0/\sin\alpha$) and minor axis ($2r_0$) [13]. The stagnation point is determined by using the theoretical analysis described by [13]. According to this theory, the stagnation point is considered as separation streamline with the section of the impingement region.

The distance between the stagnation point and the origin of the jet is calculated using ($r_0\cot\alpha$) equation. The origin of the polar radius (r_ψ) is assumed at the stagnation point (S) and the boundary of the spreading profile is defined with respect to the polar radius and azimuthal angle (ψ), as shown in Figure 2. Wang et al. [14] examined the flow patterns of horizontal and oblique liquid jets impinging on the vertical surface and reported the wetting of the surface is a dominant factor on the flow patterns. They performed the experiments with bigger inclination angles than

45° using the hydrophilic surfaces, which had 39 and 72.5° contact angles and introduced a theoretical equation for radius of the film jump with respect to the azimuthal angle, as given in Eq. (1). Since the flow pattern in the rope (rim) is complex, they suggested multiplying the jump radius with 4/3 and 2 for high and low flowrates, respectively to find the polar radius of the outer profile empirically. Therefore, the 4/3 is used to find outer polar radius in order to check the validity of this equation at the experimental conditions (e.g. θ, α), in the present study.

$$r(\Psi)_{jump} = \left(\frac{9}{50}\frac{\sin^9\alpha v_{jet}^3}{(1+\cos\alpha\cos\Psi)^6}\frac{r_0^6\rho^2}{\mu\gamma(1-\cos\theta)}\right)^{1/4} \quad (1)$$

where ρ, μ and γ are density, dynamic viscosity and surface tension of the liquid, respectively; v_{jet} is velocity of the liquid jet.

Aouad et al. [15] examined the outer spreading profile of the impinging liquid jet on the hydrophobic (θ>90°) surface by using the 3 different theory for 4 zone. In the present study, this profile is examined by using the unique one empirical equation with the governed non-dimensional numbers and the results are compared with the theory, which was introduced by [14] and [15].

The spreading profiles of the impinging liquid jet on the hydrophobic surfaces have been examined experimentally. The predicted equation has been introduced based on the experimental results. The scope of this study is that to introduce a unique global empirical equation to determine the spreading profile, maximum width, and spreading length of the impinging liquid jet on the hydrophobic surfaces.

2. EXPERIMENTAL MATERIALS AND METHODS

The distilled water was pumped from a tank to a glass tube as a nozzle with 1.75 mm inner diameter. The flowrates were adjusted using the precision needle valve and measured by the flowmeter. The nozzle was attached by a rotatable clamp, and thus inclination angles were adjusted with this clamp. The distance between the nozzle and surface was kept at ~5 mm during the experiments in order to avoid a break-up of a jet. Three different flat and smooth Teflon sheets, which had 93, 104 and 117° contact angles, were used as hydrophobic surfaces, as shown in Figure 1. These surfaces were attached on the plexiglass sheet using the two-sided adhesive tape and located vertically. Liquid jet is pumped on the surface with the inclination angles in the range of 15−45°. Distilled water was used for the liquid jet during the experiments. The images of the spreading liquid on the surface were recorded to the computer using a CCD camera. These images were analysed to define boundary profile of the liquid. The projection areas were considered for the definition. Otherwise, the wetted areas were slightly smaller than projection area because of the contact angle.

Figure 1. The contact angles of liquid droplets on the hydrophobic surfaces.

The images were analysed to determine the boundary of the spreading liquid, as shown in Figure 3. The seventeen azimuthal angles (Ψ) were used to define polar radius $r(\Psi)$ around the stagnation point, including 0, 15, 30, 45, 60, 75, 90, 105, 120, 135, 150, 155, 160 165, 170, 175, 180°, as shown in Figure 3. Half of the boundaries were used for polar radius since they were symmetrical. Boundaries of the all data were determined and these data were used to define spreading profile using a unique equation. The least-square method was employed to fit the

experimental data to a straight line. Figure 4 shows the accuracy of the Eq. (2). Mean relative percentage error was 10.2 with the limitation of the dimensionless groups as follows; Re:1800−6000, We:20−300, α:15−45° θ:93−117°. The spreading profile was investigated dependent on this accuracy.

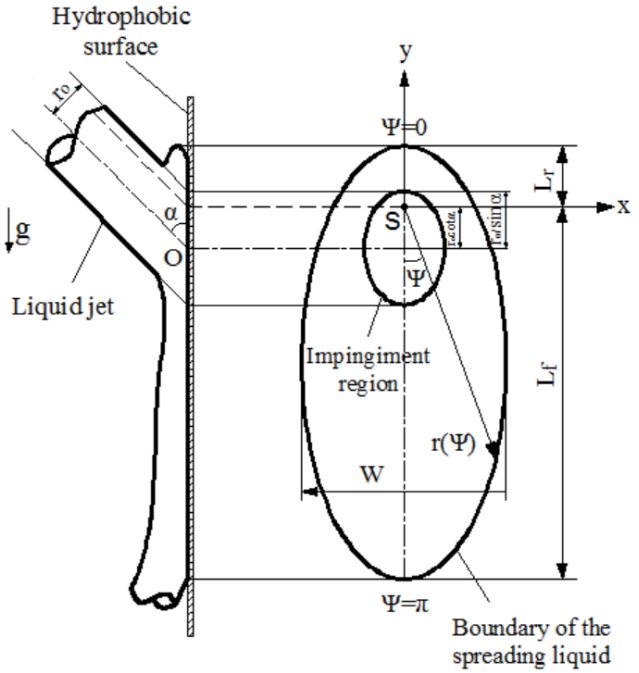

Figure 2. Schematic profile of the impinging oblique liquid on the hydrophobic surface.

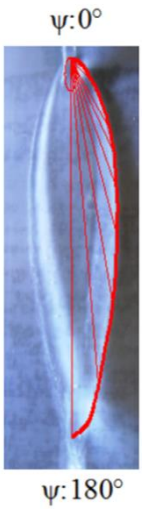

Figure 3. Azimuthal angles which used to determine the profile of the spreading liquid.

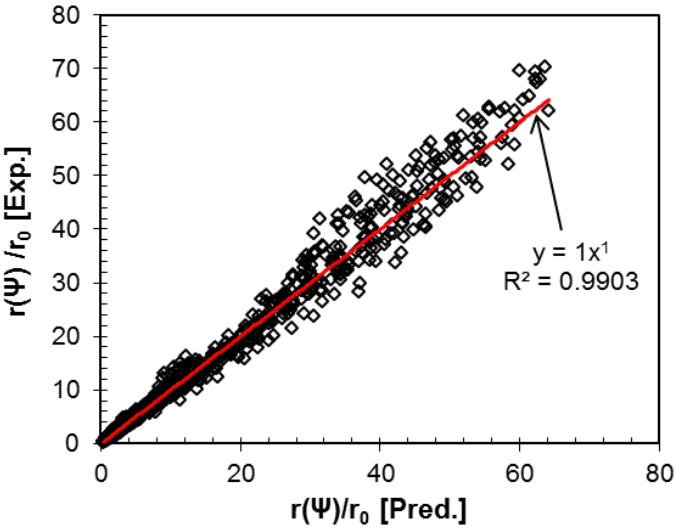

Figure 4. Comparison of the experimental profile of the spreading liquid with predicted by Eq. (2).

3. RESULTS AND DISCUSSION

In order to determine the spreading profile of the impinging liquid jet on the hydrophobic surfaces, several experiments are carried out and the experimental data are compared with the predicted model in the present study. In addition, both of the data are also compared with the theoretical model, which was introduced by [14]. The maximum spreading width, rear and front lengths with respect to the stagnation point were also analysed using the predicted equation. Therefore, the profile, maximum width, and rear/front lengths of the spreading liquid will be determined using a unique global empirical equation. Figure 5 shows an example of the predicted profile on an experimental result.

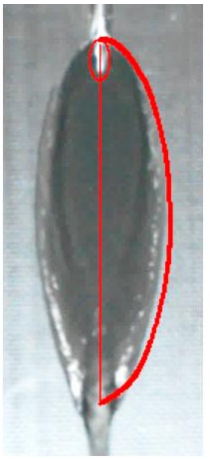

Figure 5. The comparison of the predicted and experimental results.

3.1. Spreading Profile

When a liquid jet impinges on a hydrophobic surface at an angle, it spreads on the surface around the stagnation point. The lateral extension of the liquid is limited by the surface tension and spreading liquid gathers together at a certain distance from the stagnation point [5]. Therefore, the impinging jet forms close to an elliptical shape on the surface. The spreading profile and behaviour (reflection, braiding etc.) are mainly determined with respect to the contact angle of the surface, inclination angle of the jet and physical properties of the liquid.

The outer profile of the spreading liquid is described by Eq. (2) using the governing non-dimensional variables of the flow, including the Weber number (We), Reynolds number (Re), contact angle (θ), inclination angle (α) and azimuthal angle (ψ). It is obtained by regression analysis of experimental data. The length of the spreading liquid is defined using the rear (L_r) and front length (L_f) with respect to stagnation point, as shown in Figure 2. The polar radiuses related to azimuthal angles are defined as a Cartesian coordinates using the Eqs. (3) and (4). The profile of the spreading liquid is predicted by empirical equation based on the experimental data, and it is considered with respect to stagnation point between the azimuthal angle 0 to π (Figure 2).

$$\frac{r(\Psi)}{r_0} = 0.2\mathrm{Re}^{0.3}\mathrm{We}^{0.4}[1+\cos(180-\theta)]^{-0.5}\left[\frac{(\sin\alpha)^{2.2}}{(1+\cos\alpha\cos\Psi)}\right]^{1.34}\left[e^{\Psi/\Pi}\right]^{0.65} \quad (2)$$

$$x = r(\Psi)\cos(90-\Psi) \quad (3)$$

$$y = r(\Psi)\sin(90-\Psi) \quad (4)$$

Figure 6 shows the examples of the spreading profile at different Weber numbers. The spreading area increases with the increase in the Weber number. The predicted profiles are almost in a good agreement with the experimental data. The inclination angle is a dominant factor for the profile, namely for the width and the length of the spreading liquid. If the inclination angle is low, the less liquid is directed to the upward from the impact zone results in the L_r will be low. If the jet angle is increased, the more liquid will be directed to the upward results in the bigger L_r. There are two components of the liquid jet velocity. First one is perpendicular to the surface and the other one is parallel to the surface. Liquid velocity component parallel to the surface is high at the low jet angle. Therefore, the length of the spreading profile is bigger than width since the inclination angle is lower than 45° in the present study.

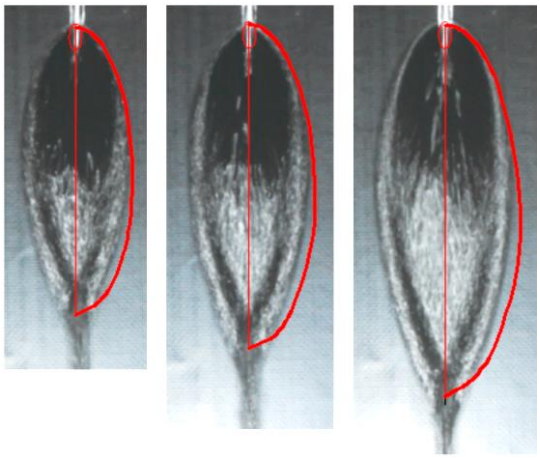

Figure 6. The spreading profile of the impinging liquid jet, α:30°, We:134, 170 and 232.

3.2. Spreading Width

The widest location of the spreading is important for cleaning and wetting applications [14]. Accordingly, the widest (maximum) widths are examined depends on the We number, inclination angle and contact angle in the present study.

Figure 7 shows the variation of the half-width of the spreading liquid with the azimuthal angles. The horizontal axis of the polar radius (x) increases with the increase in the azimuthal angle and after the maximum value it starts to decrease. This maximum value represents the maximum half-width of the spreading liquid. As it can be seen in Figure 7, the maximum width increases with the increase in the inclination angle, that means the liquid spreads a larger area laterally on the surface. However, the widest width occurs at the different azimuthal angle for the different inclination angle. The azimuthal angles, of which are occurred the maximum half-width (widest width), decreases with the inclination angle. These outcomes are also supported by the equation introduced by [14], as seen in Figure 7. In addition, the azimuthal angles, of which are occurred at maximum widths, are almost obtained the same for both equations.

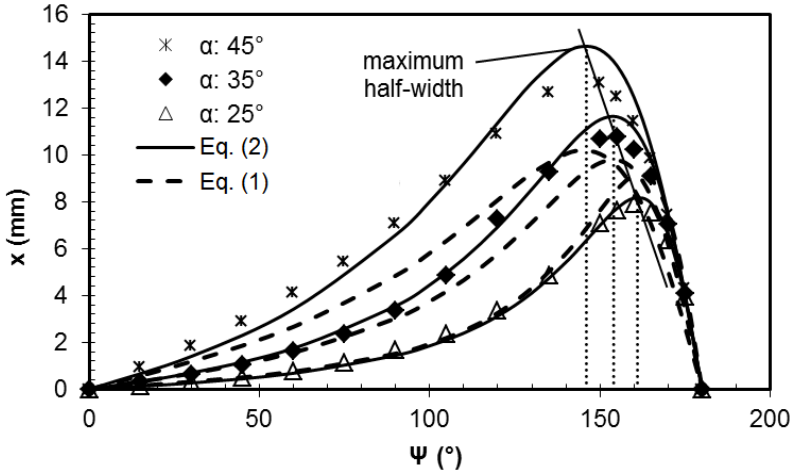

Figure 7. The half-width of the spreading liquid for different inclination angles. y axis represents the horizontal component of the azimuthal angle.

Figure 8 shows the variation of the half-width of the spreading liquid with the azimuthal angles at the different Weber number. All geometrical variables of the spreading liquid (spreading area, length, and width) increase with the increase in the We number. However, the azimuthal angles, which are occurred at the widest width, aren't affected by the Weber number, as seen in Figures 8a and 8b. This outcome is also supported by the theory, which was introduced by [14]. These results suggest that the inclination angle is a dominant factor for the spreading shape of the impinging liquid on the hydrophobic surfaces.

3.3. Spreading Length

Figure 9a shows the length of spreading liquid including the front (L_f) and rear (L_r) lengths, obtained by Eq. (2). To obtain the L_r and L_f, 0 and 180° are used for the azimuthal angle (ψ) in Eq. (2), respectively. Both the front and the rear lengths increase with the increase in the inclination angle at the beginning. However, the increasing rate decreases and increases with the tilt angle for the L_f and L_r, respectively. On the other hand, the L_f reaches a maximum value at

~33° inclination angle and then decreases with further increase in inclination angle after this value, as seen in Figure 9a. Although both the L_f and L_r increase with the increase in We number, the inclination angle, which the maximum reachable value of the L_f, isn't affected by the We number, as seen in Figure 9a.

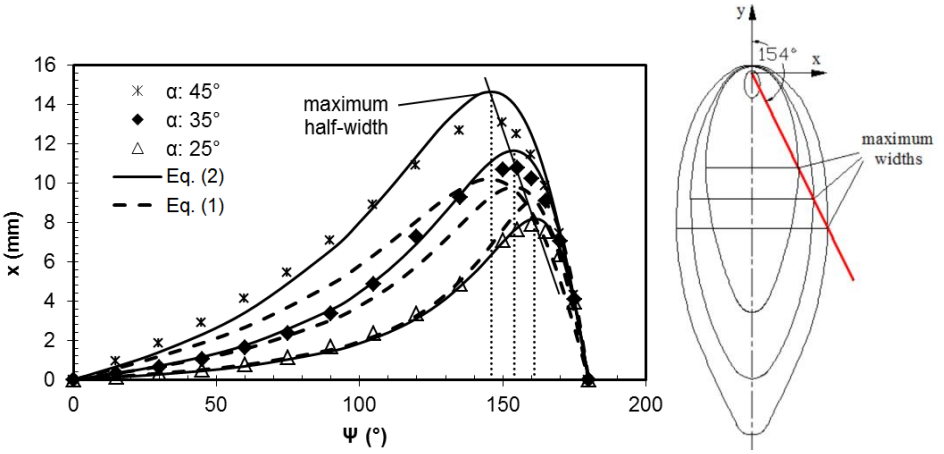

Figure 8. The maximum width of the spreading liquid at different We number, θ=117°.

With increasing the inclined angle, the tangential velocity component of the liquid jet decreases while the normal velocity component of the liquid jet increases. L_r increases due to with the increase in the normal component of the liquid jet. However, L_f is affected by the width of the spreading liquid indirectly. The kinetic energy of the liquid jet is transformed to the surface energy when the impinging liquid jet spreads on the surface [6]. Some of the kinetic energy is dissipated due to viscous and skin friction forces. Therefore, at the maximum width this transformation is altered and the spreading liquid is gathered after the maximum width owing to surface tension of the liquid. Thus, the spreading liquid reaches its maximum width far away from the stagnation point both vertically and laterally with increasing the inclination angle, and the vertical gathering distance of the liquid increases. These two results indicate why the L_f increases with the inclined angle in the range of 0 to maximum value, although the tangential velocity component of the liquid jet, which is effective for L_f, decreases.

On the other hand, the kinetic energy of the liquid jet isn't affected by the inclination angle of the jet since the energy is scalar. However, the spreading kinetic energy decreases with the transformation of the surface energy by the increasing of the spreading area, which increases with the inclination angle. Besides, the viscous dissipation increases as well. Consequently, no excess vertical inertia of the liquid remains to lengthen the spreading liquid after the critical inclination angle. The L_f is not supported by the theory, which was introduced by [14], as seen in Figure 9b. Wang et al. [14] considered the polar radius between the azimuthal angle 0 to 90°, namely they examined the profile up to the maximum width. Therefore, their theory is almost agreed with the present study only for considering the width of the spreading liquid. In order to examine profile of the jet, the theory which was introduced by [14], is valid for the width and diminish for the length.

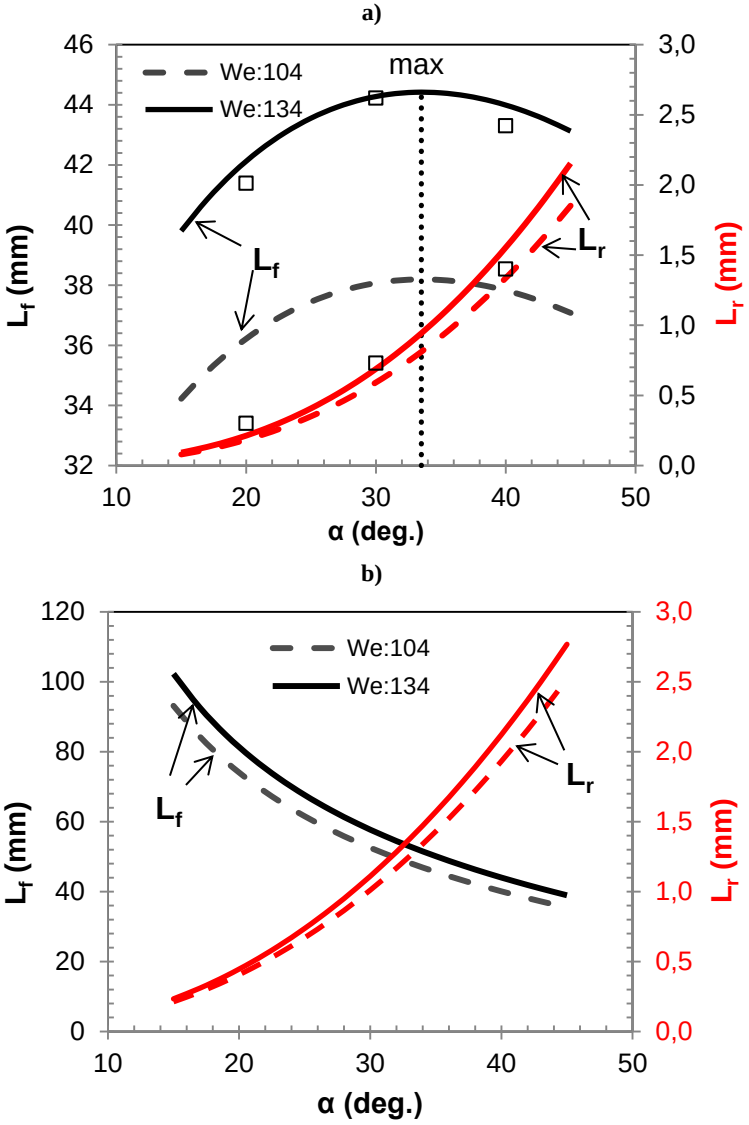

Figure 9. Front and rear lengths of the spreading liquid on the hydrophobic surface, θ:117°, a) present study b) Wang et al. [14].

4. CONCLUSION

The spreading boundary profiles of the impinging liquid jets on the hydrophobic surfaces have been examined. The outer contours are predicted empirically and the empirical equation is compared with the theory in the literature for the hydrophilic surfaces.

The azimuthal angles, where the widest widths occurred, are only affected by the inclination angle. The forward length of the spreading profile of the impinging liquid jet increases with the

increase in the inclination angle and takes a maximum value at a critical angle. It decreases with further increase in the inclination angle. This critical angle also is not affected by the Weber number. The theory in the literature is in a good agreement with the predicted equation in the study for the azimuthal angle, where the widest widths occurred.

REFERENCES

[1] Moulson JBT, Green SI (2013) Effect of ambient air on liquid jet impingement on a moving substrate. Phys Fluids 25:102106.

[2] Wang T, Davidson JF, Wilson DI 2015) Flow patterns and cleaning behaviour of horizontal liquid jets impinging on angled walls. Food Bioprod Process 93:333–42.

[3] Craik ADD, Latham RC, Fawkes MJ, Gribbon PWF (1981) The circular hydraulic jump. J Fluid Mech 112:347–62.

[4] Maynes D, Johnson M, Webb BW (2011) Free-surface liquid jet impingement on rib patterned superhydrophobic surfaces. Phys Fluids 23:52104.

[5] Kibar A, Karabay H, Yiğit KS, Ucar IO, Erbil HY (2010) Experimental investigation of inclined liquid water jet flow onto vertically located superhydrophobic surfaces. Exp Fluids 1135–45.

[6] Kibar A (2016) Experimental and numerical investigations of the impingement of an oblique liquid jet onto a superhydrophobic surface: energy transformation. Fluid Dyn Res 48:015501.

[7] Kibar A (2017) Experimental and numerical investigation of liquid jet impingement on superhydrophobic and hydrophobic convex surfaces. Fluid Dyn Res 49:015502.

[8] Kibar A (2018). Experimental and numerical investigation on a liquid jet impinging on a vertical superhydrophobic surface: spreading and reflection. Prog Comput Fluid Dyn An Int J 18:150–63.

[9] Mertens K, Putkaradze V, Vorobieff P (2005) Morphology of a stream flowing down an inclined plane. Part 1. Braiding. J Fluid Mech 531:49–58.

[10] Bush JWM, Hasha AE 2004 On the collision of laminar jets: fluid chains and fishbones. J Fluid Mech 511:285–310.

[11] Bremond N, Villermaux E (2006) Atomization by jet impact. J Fluid Mech 549:273.

[12] Inamura T, Shirota M (2014) Effect of velocity profile of impinging jets on sheet characteristics formed by impingement of two round liquid jets. Int J Multiph Flow 60:149–60.

[13] Kate RP, Das PK, Chakraborty S (2007) Hydraulic jumps due to oblique impingement of circular liquid jets on a flat horizontal surface. J Fluid Mech 573:247–63.

[14] Wang T, Faria D, Stevens LJ, Tan JSC, Davidson JF, Wilson DI (2013) Flow patterns and draining films created by horizontal and inclined coherent water jets impinging on vertical walls. Chem Eng Sci 102:585–601.

[15] Aouad W, Landel JR, Dalziel SB, Davidson JF, Wilson DI (2016) Particle image velocimetry and modelling of horizontal coherent liquid jets impinging on and draining down a vertical wall. Exp Therm Fluid Sci 74:429–43.